The Effect of Energetic Particles on Resistive Wall Mode Stability in MAST

IT Chapman[1], MP Gryaznevich[1], DF Howell[1], YQ Liu[1] and the MAST Team

[1] EURATOM/CCFE Fusion Association, Culham Science Centre, Abingdon, Oxfordshire OX14 3DB, United Kingdom

E-mail: ian.chapman@ccfe.ac.uk

Abstract. Resistive wall mode stability limits have been probed by MHD spectroscopy and numerical modelling. MAST plasmas have operated up to $\beta_N = 5.7$, well above the predicted ideal kink no-wall limit or measured resonant field amplification limits due to a combination of rotation and kinetic damping. By varying the density, both the rotation and the fast ion distribution function have been changed dramatically. Detailed drift kinetic modelling shows that whilst the contribution of energetic beam ions to resistive wall mode damping does increase at sufficiently high plasma rotation as to allow resonance with the fast ion precession frequency, the thermal ion damping always dominates over the fast ion contribution.

1. Introduction

In order to operate a future fusion power plant at an optimal cost of electricity it is necessary to develop a plasma scenario which optimises the ratio of the plasma energy to the magnetic field energy (ie maximise β where $\beta = 2\mu_0\langle p\rangle/B_0^2$ and $\langle p\rangle$ is the volume-averaged plasma pressure and B_0 is the equilibrium toroidal magnetic field) whilst simultaneously minimising the amount of power required to supply the current non-inductively. Indeed, the EU Power Plant Conceptual Study (PPCS) [1] concluded that in order to produce electricity at economically attractive rates in a future fusion power plant, plasma performance beyond the ITER baseline level [2] is required [3]. One goal of ITER [2] is to demonstrate reactor-scale steady-state tokamak operation. 'Advanced tokamak scenarios' [4–8] maximise the self-generated non-inductively driven bootstrap current [9] through a combination of operating at high plasma pressure and low plasma current. However, such plasma parameters make the discharges more susceptible to deleterious magnetohydrodynamic (MHD) instabilities which would not be unstable with conventional H-mode profiles [10, 11]. The ultimate performance limit in advanced tokamak scenario operation is often set by the resistive wall mode (RWM). The RWM is a macroscopic pressure-driven kink mode, whose stability is mainly determined by damping arising from the relative rotation between the fast rotating plasma and the slowly rotating wall mode. In the absence of a surrounding wall, the plasma is stable to kink modes until the normalised plasma pressure, $\beta = 2\mu_0\langle p\rangle/B^2$, exceeds a critical value, β_∞. In the presence of an ideally conducting wall, the plasma is stable to a critical value, β_b, with the range $\beta_\infty < \beta < \beta_b$ called the wall-stabilised region. In practice, the vessel wall has a finite resistivity. Thus, on the time scale required for eddy currents to decay resistively, the magnetic perturbation of the external kink mode can penetrate the wall and so wall-stabilisation is lost.

It has been shown in a number of machines that the plasma can operate above the no-wall β-limit [12–19], even with very low rotation [20–23]. Recent experiments with nearly balanced neutral beam injection (NBI) [20, 21] have found a critical velocity for RWM stabilisation well below that found in previous magnetic braking experiments [19]. Consequently, in order to make reliable extrapolation to ITER performance, it is crucial to understand the passive stabilisation allowing operation above the predicted no-wall stability limits. Various models have been presented to explain the RWM damping due to kinetic effects, such as sound-wave damping [24], ion Landau damping [25], or damping arising from resonance with the precessional drift of thermal ions [26, 27]. Numerical simulation has shown that the damping from resonance with the precession frequency of thermal ions [28–30] or fast ions [31, 32] can significantly raise the RWM stability limit. In order to explicate the effects of energetic ions in determining the RWM stability limits, dedicated experiments with different fast ion distributions have been performed in MAST plasmas operated well above the ideal no-wall stability limit predicted by either linear stability analysis (where rigorous equilibrium reconstruction has been shown to be highly accurate in the saturated internal mode onset studies in

ref [33]) or from the resonant field amplification limit, which is understood to provide information on the no-wall limit [34]. In order to test whether significant damping is caused by the NBI fast ions, the plasma response has been measured for a range of fast ion distributions – achieved by varying plasma density – and compared to the damping rate. In section 2 the experimental measurements of proximity to RWM stability limits are presented for plasmas with different NBI fast ion populations. The distribution of the fast particles is assessed in section 3 and used to consider the kinetic damping effects on the external kink mode in these MAST plasmas in section 4. Finally, conclusions and implications for RWM stability limits are discussed in section 5.

2. Resonant Field Amplification Experiments in MAST

A weakly damped mode, such as the RWM in the presence of rotation or kinetic damping, can amplify the resonant component of magnetic field asymmetries [35]. This means that RWM stability can be probed experimentally by examining the plasma response to externally applied non-axisymmetric magnetic fields. When the plasma pressure exceeds the no-wall β-limit, strong resonant field amplification (RFA) of the applied field occurs, meaning that RFA can be used to infer the ideal no-wall β-limit. The measured frequency spectrum of the RFA to externally applied rotating magnetic fields has been described by a single-mode approach [34]. This allows an absolute measurement of the damping rate and natural mode rotation frequency of the RWM.

The resonant field amplification amplitude is usually defined as the ratio of the plasma response to the externally applied field, B_r^{ext}. It is found by measuring the perturbed radial magnetic field at sensors at the wall, B_r, and is defined as

$$A_{\text{RFA}} = \frac{B_r(r = r_{\text{sensor}}) - B_r^{\text{ext}}}{B_r^{\text{ext}}} \tag{1}$$

The resonant field amplification, A_{RFA}, is a complex number, whose phase angle refers to the toroidal phase of the plasma response with respect to the externally applied field [34]. More recently, differences between the RFA limit and the no-wall β-limit in JET have been negated by redefining the RFA limit as the β value at which the logarithmic derivative of the measured RFA as a function of β_N reaches a maximum [36].

In MAST, oscillating non-axisymmetric magnetic fields have been applied from the internal coils, consisting of two rows of six coils mounted inside the vacuum vessel, equally spaced toroidally and located symmetrically above and below the midplane. The coils are made of four turns and equipped with power supplies that can provide 1.4kA in each turn. In these experiments, toroidally opposite coils are connected in series with oppositely directed currents to produce an $n = 1$ field. The external field has been applied in identical plasma discharges with frequency varying from 30Hz to 100Hz in the same direction as the plasma rotation. By measuring the plasma response on pairs of saddle coils, both in the same sectors of the vessel as the internal coils from which the magnetic perturbation is applied, and also in sectors orthogonal to the applied field, the amplitude of the RFA can be found. B_r^{ext} was measured in a series of vacuum

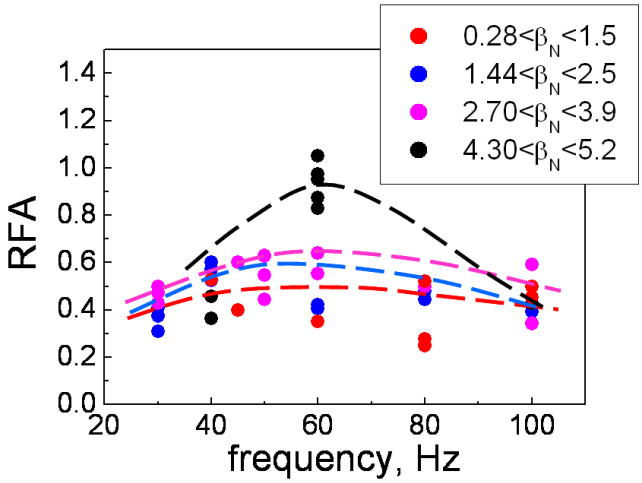

Figure 1. The resonant field amplification amplitude as a function of applied oscillating field frequency. It is apparent that the clearest amplification is observed when the applied field is at 60Hz.

only discharges, and the saddle coil data are corrected by subtracting the signal from a plasma with no applied field in order to remove direct pick up from the poloidal field coils. It should be noted that due to noise in the saddle coil signals, the raw data have been bandpass filtered by ±4Hz around the applied frequency and the RFA calculated for any given β_N over three cycles. A cross-correlation between the RFA signal produced and the applied current is then performed, and data are only retained if the coherence is above a threshold of 0.8. The RFA in a series of MAST discharges for a range of β_N with various applied field frequencies is illustrated in figure 1. It is evident that the RFA is maximised at an applied field of 60Hz, and so all measurements during β_N scans are performed at this frequency.

In order to assess the effect of the fast ions on the plasma stability limits, the fast ion distribution function has been varied by changing the plasma density. By changing the density, the fast ion gradients in both radial and velocity space will change. As the density increases, the fast ion population becomes broader in radius and more peaked in energy. Whilst different density would nominally lead to a different q-profile, which implicitly affects global stability, the density scan was performed in deliberately vertically-displaced MAST plasmas in order to keep the q-profile relatively constant. By down-shifting the plasma, the neutral beam deposition is shifted off-axis, avoiding the strongly stabilising effect on the internal kink mode of a fast ion population peaked on-axis [37,38]. In a spherical tokamak, where the broad low-shear core q-profile typically results in $r_{q=1}/a \geq 0.5$, a significant fraction of energetic ions inside the $q = 1$ surface can stabilise the first sawtooth to the extent that it is disruptive. Operating in single null and moving the beam distribution off-axis permitted access to high β_N

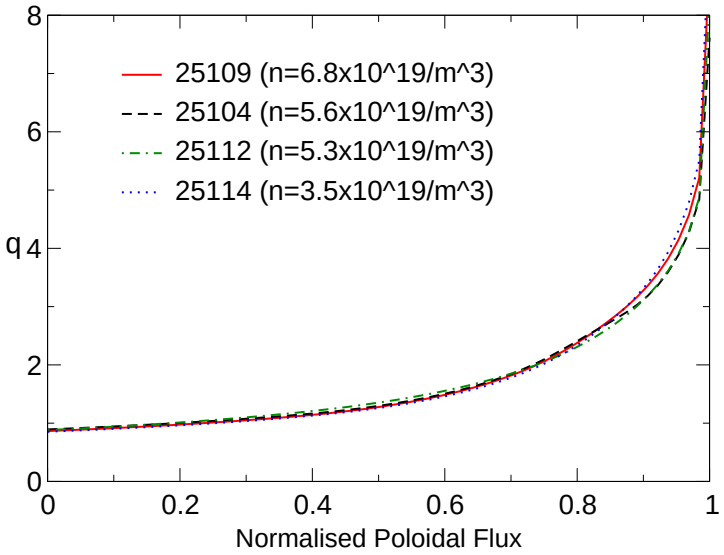

Figure 2. The safety factor profile at $t = 0.3$s for four MAST plasmas with varying plasma density, namely 25109 ($n_e = 6.8 \times 10^{19} m^{-3}$), 25104 ($n_e = 5.6 \times 10^{19} m^{-3}$), 25112 ($n_e = 5.3 \times 10^{19} m^{-3}$) and 25114 ($n_e = 3.5 \times 10^{19} m^{-3}$).

since the sawteeth are small and regular. These frequent sawteeth also mediate the safety factor evolution and consequently the q-profile is approximately constant despite significant changes in the density. Figure 2 shows clearly that the q-profile calculated by EFIT equilibrium reconstruction is barely changed by the scan in plasma density. Here the EFIT reconstruction is constrained by measurements of the magnetic field pitch angle from the Motional Stark Effect (MSE) diagnostic, electron temperature and density profiles from the high resolution Thomson Scattering (TS) diagnostic and D_α measurements to constrain the edge of the plasma. Unfortunately, vertically displacing the plasma is sub-optimal for some of the diagnostic systems whose line-of-sight is along the vessel midplane, but sufficiently detailed equilibria can still be reconstructed.

Increasing the density results not only in the fast ion distribution becoming peaked further off-axis and at lower energies, but also the rotation velocity increases, which pertinently affects RWM stability. However, the fast ion orbit width (which is significant in spherical tokamaks, $\Delta_r/a \approx 0.2$ and can play a significant role in RWM stability [39]) remains approximately the same, which is not the case using an alternative experimental approach of varying I_p/B_t in order to change fast ion confinement whilst keeping q the same [32].

Figure 3 shows plasma parameters of a typical MAST plasma in the middle of the density scan. During the discharge the neutral beam heating power is increased and then the plasma current is ramped down from 600kA to 500kA in order to progressively increase β_N, allowing the plasma response to be measured for different values of plasma pressure. The toroidal magnetic field is held fixed at $B_t = 0.5$T and the electron density is varied in the range $n_e \in [3.0, 6.8] \times 10^{19}\mathrm{m}^{-3}$. The oscillating external field is applied at 60Hz in H-mode plasmas which reach $\beta_N \sim 5.5$, and exceed the ideal no-wall MHD

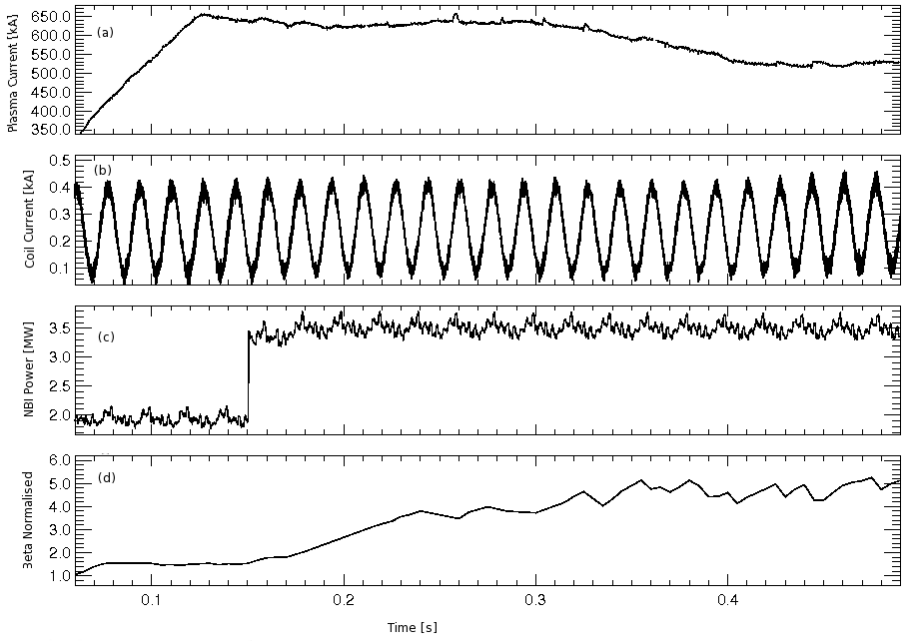

Figure 3. (a) The plasma current; (b) The applied oscillating field; (c) The injected NBI power and (d) β_N calculated by EFIT for MAST discharge 25105.

stability limit predicted by linear MHD stability analysis using the MISHKA-1 code [40]. As the NBI power is increased, the toroidal rotation increases too, which together with the kinetic effects discussed in section 4, means that the plasma operates above the no-wall limit without the RWM becoming unstable.

Although the RWM is stable in these MAST plasmas, an increase in resonant field amplification can be viewed as a proxy for the ideal no-wall stability limit [36, 41]. The RFA is measured for a series of MAST plasmas with different density, and thus different fast ion distributions and different rotation profiles, but ostensibly identical q-profiles and fast ion orbit widths. Figure 4 shows the RFA measured by midplane saddle coils with respect to the β_N calculated by EFIT equilibrium reconstruction for five MAST plasmas. The RFA limit is seen at approximately the same β_N for a range of different densities, confirming that the plasma parameters that dominate ideal fluid stability are essentially unchanged. However, in all cases, the plasma is able to operate above the RFA limit, due to a combination of rotation stabilisation and kinetic damping.

Whilst the RFA only predicts the no-wall limit, it is possible to infer the plasma response to the externally applied oscillating external field by using a simple single mode model [34], which can then be directly compared to quantification of the mode damping rate from numerical assessment. The plasma response at the wall is given by

$$\delta B_{s,plasma} = \frac{M^*_{sc}(\gamma_0\tau_w + 1)I_c}{(i\omega_{ext}\tau_w - \gamma_0\tau_w)(i\omega_{ext}\tau_w + 1)} \tag{2}$$

where γ_0 is the growth rate of the RWM in the absence of applied fields, I_c is the current

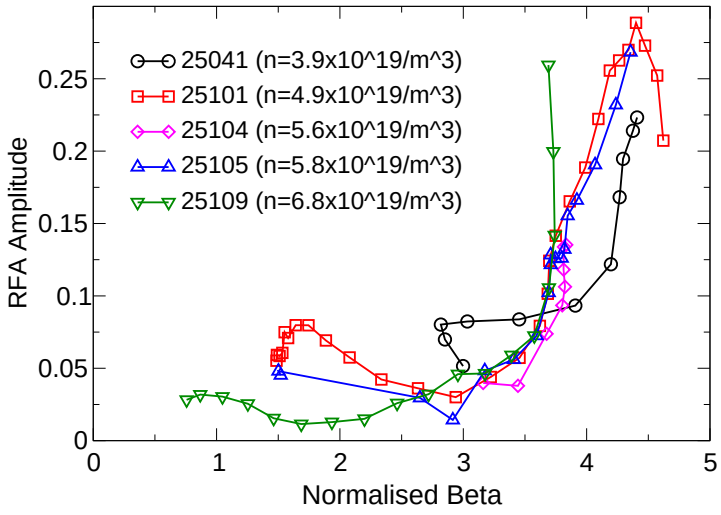

Figure 4. The RFA amplitude as a function of β_N for five MAST discharges with different plasma density, namely 25109 ($n_e = 6.8 \times 10^{19} m^{-3}$), 25104 ($n_e = 5.6 \times 10^{19} m^{-3}$), 25105 ($n_e = 5.8 \times 10^{19} m^{-3}$), 25101 ($n_e = 4.9 \times 10^{19} m^{-3}$) and 25041 ($n_e = 3.9 \times 10^{19} m^{-3}$. The no-wall stability limit is taken to be where the RFA begins to markedly increase as the mode approaches marginal stability.

in the perturbing external coils, τ_w is the characteristic resistive decay time for currents in the wall induced by the RWM and M^*_{sc} is the effective mutual inductance describing the direct coupling between the coils and the resonant component of the externally applied field at the wall. It is possible to fit the free parameters γ_0 and M^*_{sc} to the measured RFA as a function of the frequency of the applied magnetic field. Figure 5 shows the RFA as a function of applied frequency with the amplitude of the RFA fit according to [34]

$$A_{RFA} = -\frac{M^*_{sc}}{M_{sc}} \frac{1 + \gamma_0 \tau_w}{\gamma_0 \tau_w} \tag{3}$$

where M_{sc} is the externally applied field detected by the saddle coil sensors and the wall time $\tau_w = 37.5$ms is found from vacuum response data. Having found the γ_0 and M^*_{sc} free parameters by fitting the frequency-dependence of the RFA to equation 3, the plasma response to the applied fields can be found using equation 2. Comparison of the plasma response to the damping rate found by detailed modelling is given in section 4.

3. Equilibria and fast ion distributions

Equilibria have been reconstructed for a number of timeslices as the β_N increases during each MAST discharge with a different plasma density. The equilibria are generated using the HELENA code [42] which is supplied with the EFIT [43] equilibrium and constrained by the position of the $q = 1$ surface from the measured inversion radius observed in the soft X-ray emission. The EFIT equilibria are constrained by the MSE measurement of the magnetic field pitch angle and the TS measurement of the electron density and

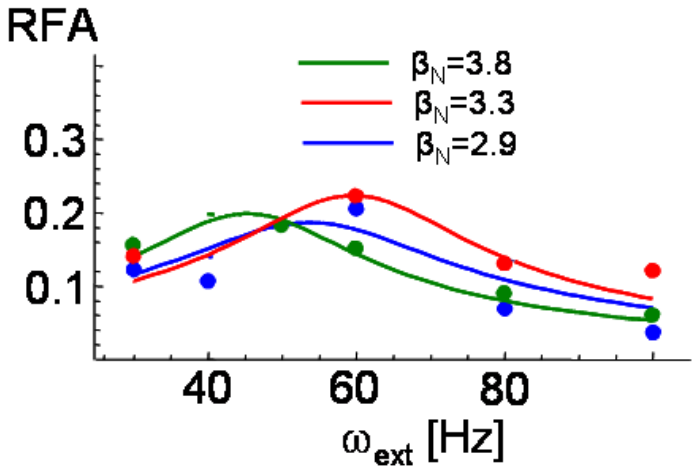

Figure 5. The RFA amplitude (symbols) as a function of applied field frequency for three different plasma pressures. Shown for comparison (lines) is the RFA amplitude predicted by equation 3, used to ascertain the free parameters γ_0 and M_{sc}^*.

temperature profiles. The current density profile is taken from TRANSP [44] calculations in order to accurately include the neutral beam driven current. Unfortunately, the MSE measures the pitch of the field lines along the path of the neutral beam, which is not near the magnetic axis in these vertically displaced MAST plasmas, resulting in a greater uncertainty in the core q-profile predicted by EFIT. However, the qualitative comparison between the discharges with different densities indicates no significant relative variation in the q-profile.

In order to facilitate modelling of the effect of the fast ions on the stability of the resistive wall mode, the fast ion distribution in phase space must be calculated. Therefore, the fast ion distribution function for the different plasmas discussed in section 2 has been assessed with the TRANSP code [44].The TRANSP code was used in these studies as it enables use of the detailed Monte Carlo beam module NUBEAM in a convenient, integrated plasma simulation environment. The beam ion distribution function integrated over all particle energies and pitch angles is shown in poloidal cross-section for four MAST plasmas with varying plasma density in figure 6. In all cases the fast ion population is peaked off-axis, though well inside the $q = 2$ surface which plays an important role in determining RWM stability. Incidentally, it is the off-axis nature of the fast ion distribution which produces small, frequent sawteeth [37] allowing operation at high-β_N in MAST. Figure 6 shows that as the density is decreased, the fast ion density increases by nearly a factor of two and the distribution becomes more peaked towards the axis.

Figure 7, which shows the beam ion density as a function of normalised minor radius, clearly indicates both the increase in fast ion density and the inward shift of the peak of fast ion deposition as the density is decreased. Here the fast ion distribution is integrated over all energies and pitch angles. As the density decreases, the radial

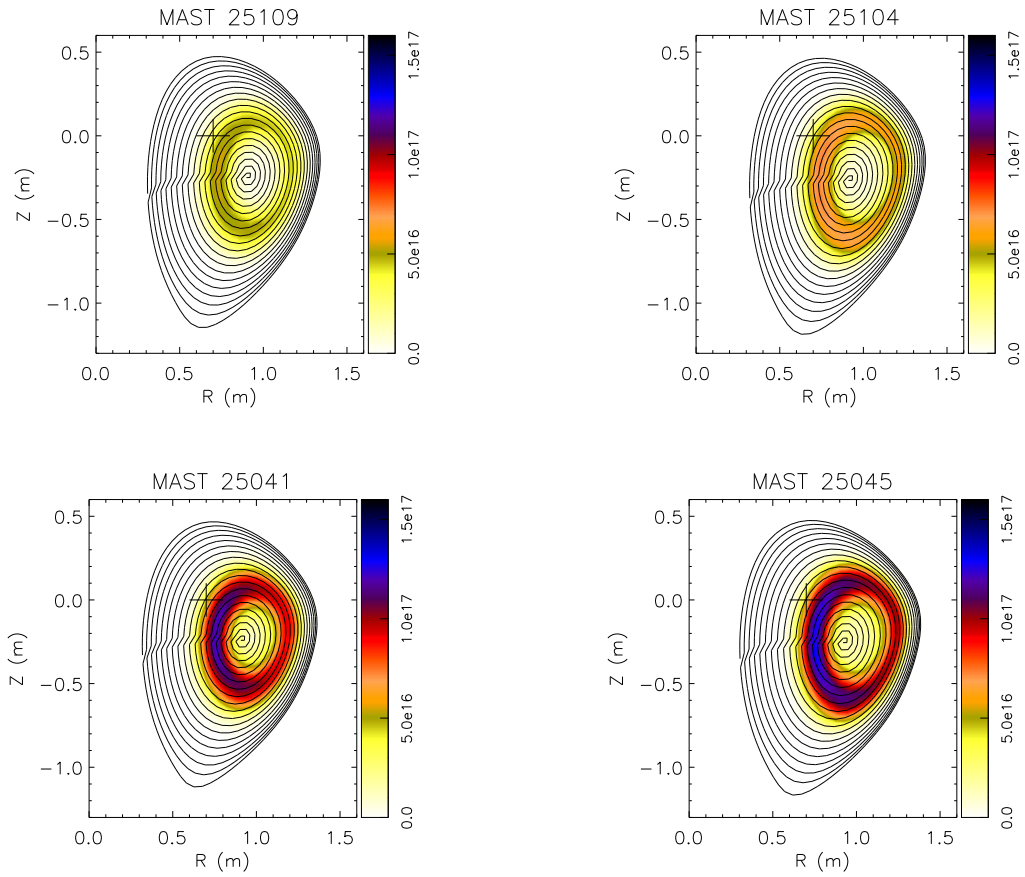

Figure 6. The NBI fast ion density at $t = 0.3$s as predicted by TRANSP for MAST discharges 25109 ($n_e = 6.8 \times 10^{19} m^{-3}$), 25104 ($n_e = 5.6 \times 10^{19} m^{-3}$), 25041 ($n_e = 3.9 \times 10^{19} m^{-3}$) and 25045 ($n_e = 3.1 \times 10^{19} m^{-3}$). As the plasma density decreases, the fast ion density increases and becomes more peaked.

gradient of the fast ion density on the high-field side of the peak of beam ion deposition does not change as much as on the low-field side of the distribution peak. This means that $\partial f_h / \partial r$ across the $q = 2$ surface changes significantly, which together with the increase in β_h is likely to strongly affect the change in the potential energy of the kink mode arising from the presence of the fast ions.

The variation in pitch angle and the trapped fraction do not change significantly with the plasma density. However, there is a significant change in the beam ion distribution as a function of particle energy as n_e changes, as illustrated in figure 8. As the density decreases, the fast ion density at higher particle energy increases, broadening the distribution function in energy space. These more energetic ions have a larger orbit width – since Δ_r increases with the parallel velocity – which is likely to lead to a stronger influence upon kink mode stability.

The final part of the plasma equilibrium which is significantly affected by the variation in plasma density is the toroidal rotation profile. Since the plasma is vertically displaced in the open MAST vessel, the angular momentum imparted by NBI heating

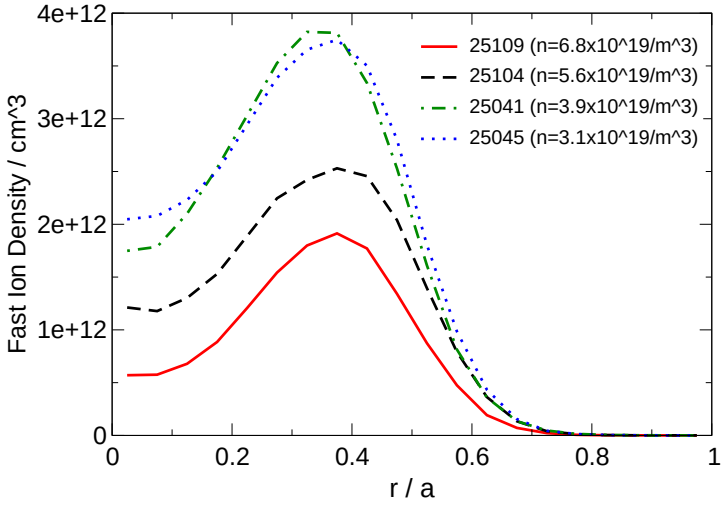

Figure 7. The fast ion density predicted by TRANSP as a function of r/a at $t = 0.3$s for four MAST plasmas, namely 25109 ($n_e = 6.8 \times 10^{19} m^{-3}$), 25104 ($n_e = 5.6 \times 10^{19} m^{-3}$), 25041 ($n_e = 3.9 \times 10^{19} m^{-3}$) and 25045 ($n_e = 3.1 \times 10^{19} m^{-3}$).

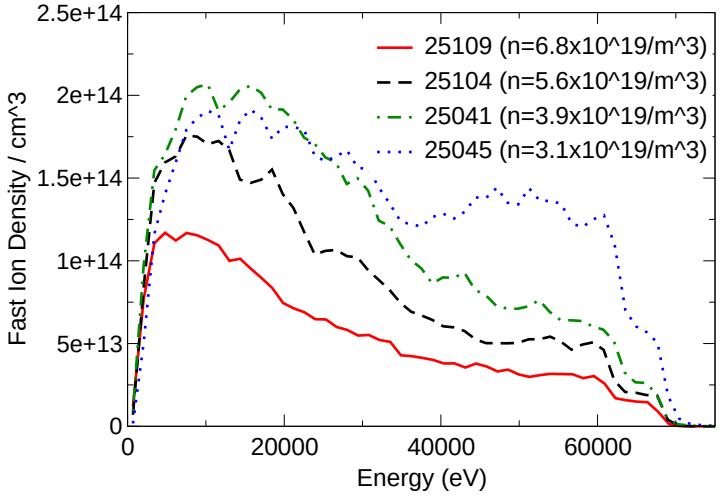

Figure 8. The fast ion density predicted by TRANSP as a function of particle energy at $t = 0.3$s for four MAST plasmas, namely 25109 ($n_e = 6.8 \times 10^{19} m^{-3}$), 25104 ($n_e = 5.6 \times 10^{19} m^{-3}$), 25041 ($n_e = 3.9 \times 10^{19} m^{-3}$) and 25045 ($n_e = 3.1 \times 10^{19} m^{-3}$).

is decreased, meaning that the plasmas studied here rotate much slower than typical double-null MAST plasmas. Such strongly sub-Alfvénic rotation speeds enhance the ITER relevance of these plasmas. Table 1 shows the plasma rotation speed relative to the Alfvén speed and the fraction of the plasma pressure contributed by the fast particles, where $v_0/v_A \leq 10\%$ and $\beta_h/\beta_{total} \leq 60\%$. As the mass density changes, the torque resulting from neutral beam injection varies and consequently the centrifugal effects on the equilibrium alter, and more importantly, the Doppler-shift of the kink mode frequency changes which strongly affects the resonant interaction between the mode and the natural frequencies of species of both thermal and energetic particles.

Shot	$n_e \times 10^{19}\mathrm{m}^{-3}$	v_0/v_A	β_h/β_{total}
25109	6.8	0.103	0.091
25104	5.6	0.070	0.167
25041	3.9	0.046	0.337
25045	3.1	0.012	0.589

Table 1. Table giving the plasma velocity normalised to the Alfvén velocity and the fast particle contribution to the β normalised to the total β for MAST plasmas with different densities.

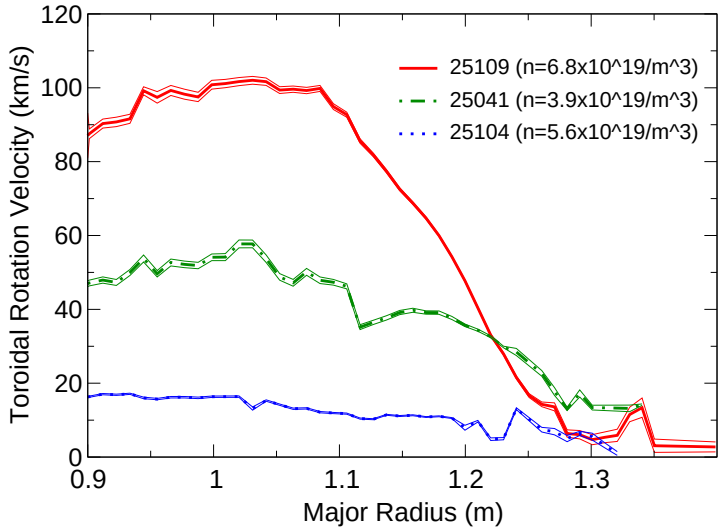

Figure 9. The toroidal rotation velocity measured by Charge Exchange spectroscopy as a function of major radius at $t = 0.3$s for three MAST plasmas, namely 25109 ($n_e = 6.8 \times 10^{19} m^{-3}$), 25041 ($n_e = 3.9 \times 10^{19} m^{-3}$) and 25045 ($n_e = 3.1 \times 10^{19} m^{-3}$). The thin bounding lines represent the error bar on the measurement. For comparison, the $q = 2$ surface from EFIT equilibrium reconstruction is at approximately $R = 1.25$m in all cases.

The toroidal rotation for three MAST plasmas of different density is shown in figure 9. At higher density, the toroidal rotation in the core is much larger. EFIT equilibrium reconstruction suggests that the $q = 2$ surface is at approximately $R = 1.25$m in all three plasmas shown in figure 9. At this radial location, the rotation frequency does not change significantly as the plasma density increases. However, subtle changes in the rotation frequency can significantly affect the particles with which the RWM is in resonance, as discussed in section 4. The stronger sheared rotation at higher density can also affect RWM stability directly [19, 45, 46].

4. Assessment of Kinetic Damping

In the MAST experiments outlined in section 2, the plasma is sustained well above the RFA limit and the calculated no-wall linear stability limit. Thus, it is important

to understand the passive stabilisation allowing stable operation in the wall-stabilised regime without direct suppression of the RWM, with a view to making reliable predictions for RWM stability in ITER and future power plants, which are predicated upon RWM avoidance [47, 48]. The earliest models for kinetic damping of the RWM were based upon parallel viscosity or sound wave damping of the mode [24, 49]. Later it was suggested that the RWM would be damped due to a resonance between the mode frequency and the transit (bounce) frequency of the passing (trapped) energetic ions in the plasma [25]. More recently, kinetic theory has also been applied to suggest that the RWM will be damped in the presence of trapped thermal ions due to a resonance between the mode and the drift precessional motion of the particles [26, 27]. In this study, the HAGIS drift kinetic code [50] has been used to compute the change in the potential energy of the kink mode in the presence of both thermal and energetic particles, $\delta W_K = \delta W_{th} + \delta W_h$. HAGIS is a particle-orbit code following the guiding centre motion of the particles, meaning that all the relevant resonances with particle motion are included rigorously. This modelling includes finite orbit width effects that have been neglected in previous studies [27, 29–31].

The growth rate of the RWM can be formulated in terms of the MHD perturbed energy, as [51]

$$\gamma\tau_W = -\frac{\delta W_\infty}{\delta W_b} \tag{4}$$

where $\delta W_{b,\infty}$ represents the sum of the plasma and vacuum energy with and without a wall respectively. Equation 4 can be extended to include the kinetic contribution to the plasma energy, δW_K, for low frequency modes [27], such that

$$\gamma\tau_W = -\frac{\delta W_\infty + \delta W_K}{\delta W_b + \delta W_K} \tag{5}$$

where $\delta W_\infty < 0$ and $\delta W_b > 0$, indicating that the plasma is in the region where the ideal external kink mode is stable, but the RWM is MHD unstable.

The change in the potential energy of the unstable mode due to kinetic effects is expressed as [52]

$$\delta W_K = -\frac{1}{2}\int \xi_\perp^* \cdot (\nabla \cdot \tilde{\mathbb{P}}_K)\mathrm{d}V \tag{6}$$

where ξ is the plasma displacement eigenfunction, $\tilde{\mathbb{P}}_K$ is the perturbed pressure tensor which can be found by taking moments of the perturbed distribution function, which itself can be found by solving the linearised drift kinetic equation, and V is phase space including both velocity and volume integrals. By solving the drift kinetic equation and substituting in for $\tilde{\mathbb{P}}_K$ then performing phase space integrals over particle energy, $\mathcal{E}$, pitch angle, $\lambda = v_\parallel/v$, and flux, ψ, it can be shown that the kinetic potential energy of the mode incorporates a frequency resonance condition [26, 32, 53],

$$\delta W_K \sim \sum_{l=-\infty}^{\infty} \frac{(\omega - n\omega_E)\partial f_j/\partial\mathcal{E} - \frac{1}{eZ_j}\partial f_j/\partial\psi}{\omega - n\omega_E + i\nu_{eff,j} - \langle\omega\rangle_{d,j} - l\omega_{b,j}} \tag{7}$$

where ω is the complex eigenmode frequency, the $E \times B$ frequency is $\omega_E = \omega_\phi - \omega_{*i}$, ω_ϕ is the toroidal rotation frequency, ω_{*i} is the ion diamagnetic frequency, Z is the effective plasma charge, e is the electron charge, the particle energy is $\mathcal{E} = v^2/2$, $\langle\omega\rangle_d$ is the orbit-averaged drift precession frequency, ω_b is the trapped-particle bounce frequency and ν_{eff} is the collision frequency. Using the HAGIS code, all of the toroidal and poloidal bounce(transit)-averaged frequencies for any species of particles can be calculated, though collisions are neglected. It is clear from equation 7 that a resonance between the Doppler shifted mode frequency and these particle frequencies can occur when the denominator vanishes. Since the natural particle orbit frequencies vary by orders of magnitude, such resonances occur with either the transit frequency of passing particles, $\omega - \omega_E \sim \omega_t \sim v/R$; the bounce frequency of the trapped particles, $\omega - \omega_E \sim \omega_t \sim \sqrt{r/R}(v/R)$; or the precession drift motion, $\omega - \omega_E \sim \omega_t \sim \rho/r(v/R)$, where $\omega_d \ll \omega_b < \omega_t$ and ρ is the Larmor radius, $\rho = mv_\perp/eB$ and $v_\perp$ is the particle speed perpendicular to the magnetic field. Whilst it has been shown that the low-frequency RWM can resonate with both the precession drift frequency and bounce frequencies of thermal ions (depending on the plasma rotation) [28–30], for energetic particles typically $\omega_d, \omega_b \gg \omega - \omega_E$. Consequently, it is likely that the contribution from the energetic particles is not a resonant process, but related to (i) an increase in the resistance to changes in the magnetic flux by the kink mode through an inhibition of toroidal coupling of harmonics and (ii) finite orbit width effects of the energetic ions. The two conditions where a resonant contribution may persist are either when the hot ions are near the trapped-passing boundary, or when they experience a toroidal precession reversal. Recent studies have suggested that neutral beam ions [32] and fusion-born alpha particles [31] are stabilising to the RWM, but that their effect is less significant than the thermal species. However, these studies used the MISK [26] and MARS-K [53] codes respectively, neither of which incorporates the radial excursion of the particles.

As observed in figure 2, the safety factor in these MAST plasmas has a wide region of low magnetic shear, extending beyond mid-radius. Consequently, these plasmas become unstable to global kink-ballooning modes at sufficiently high pressure gradients [54]. These eigenmodes do have external components which, in the absence of dissipative stabilising effects, would cause eddy currents in the toroidally continuous poloidal field coil casings which act as the wall in MAST when the plasma pressure is above the no-wall limit, allowing a RWM – albeit with an infernal mode structure [10] rather than external kink – to grow unstable. This global eigenmode is a resistive wall mode in the sense that bringing a perfectly-conducting wall sufficiently close to the plasma boundary stabilises the mode numerically.

The plasma response measurements in the MAST shots in section 2 show that the RFA limit does not vary significantly with density. Indeed, figure 4 shows that the increase in RFA always occurs in the range $\beta_N \in [3.7, 4.2]$ The ideal no-wall and with-wall stability limits of these plasmas has been tested using the MISHKA-1 linear stability code [40] after the equilibria had been reconstructed as described in section 3 at the time point at which the RFA is seen to markedly increase. Here, the wall constitutes

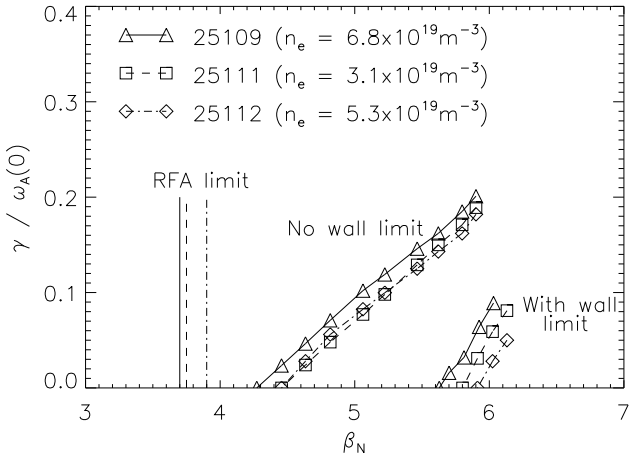

Figure 10. The RFA limit measured experimentally compared to the no-wall and with-wall ideal stability limits predicted by MISHKA linear stability analysis for three MAST plasmas, namely 25109 ($n_e = 6.8 \times 10^{19} m^{-3}$), 25111 ($n_e = 3.1 \times 10^{19} m^{-3}$) and 25112 ($n_e = 5.3 \times 10^{19} m^{-3}$).

the vacuum vessel and the toroidally-continuous conducting casings which surround the poloidal field coils. The growth rate of the limiting $n = 1$ mode as a function of β_N is shown in figure 10 and compared to the RFA limit, assessed as the normalised beta at which the RFA amplitude begins to sharply increase. It is clear that in all cases, the measured RFA limit is below the predicted ideal no-wall limit, but that across the scan in density, these two limits remain relatively constant. The small variation in the β-limits between discharges arises due to different trajectories in (β_N, q_{min}) space as the plasma evolves at different densities. Results from JET also find the RFA limit is often below the ideal no-wall limit, leading to a redefinition of the RFA limit as the β_N at which the logarithmic derivative of the RFA is maximised [36]. However, the oscillations in the MAST data illustrated in figure 4 mean that the logarithmic derivative of the RFA does not have a clear maximum, so cannot be used to infer the experimental no-wall stability limit. Nonetheless, the qualitative agreement between the RFA measurements and the linear stability analysis, coupled with similar discrepancies between the two limits in other devices, gives reasonable confidence that the modelling is an accurate representation of the β-limits in these MAST plasmas. Consequently, these calculated stability limits can be used in equation 5 to predict the damping rate of the stable RWM in these plasmas.

4.1. Role of energetic beam ions

As discussed in the previous section, few energetic ions contribute to δW_K through a resonant interaction since the mode frequency corrected by the plasma rotation $(\omega - \omega_E)$ in equation 7 only approaches the bounce or precession frequencies for high

rotation speeds. However, in a spherical tokamak two factors mean that at least a small proportion of the energetic ions can undergo a resonant interaction: Firstly, the small moment of inertia of a low aspect-ratio device coupled with the large injected neutral beam power per unit volume mean that significant rotation speeds, approaching the ion sound speed, can be achieved; secondly, the high beta inherent in an ST together with the low aspect ratio result in lower toroidal precession frequencies, meaning that $\omega - \omega_E \rightarrow \langle\omega\rangle_{d,h}$. Furthermore, at high particle energies associated with NBI ions, the gap between the bounce frequency and the precession frequency is reduced, since (approximately [55]) $\omega_b = v_\perp\sqrt{\epsilon}/\sqrt{2}qR$ and $\omega_d = qv_\perp^2/2\epsilon R^2\Omega_c$ where $\epsilon = a/R$ is the inverse aspect ratio and Ω_c is the cyclotron frequency, $\Omega_c = eB/m$, meaning that

$$\frac{\omega_b}{\omega_d} \sim \frac{r}{q^2\rho}\sqrt{\frac{2r}{R}} \tag{8}$$

In order to explicate the role of the beam ions in damping the RWM in MAST, δW_K has been calculated with HAGIS for MAST plasmas with different plasma densities as described in section 3. By using a drift kinetic code, the frequencies of all of the particles can be calculated rigorously as $\omega_\phi = \oint \phi \mathrm{d}t / \oint \mathrm{d}t$ integrating along a closed poloidal orbit and $\omega_\theta = 2\pi/\Delta t$ without making ensemble averages. Whilst the particle orbits and finite radial excursion are treated comprehensively, using HAGIS involves a perturbative approach whereby the drift kinetic modification of the RWM eigenfunction is neglected and the eigenfunction of the ideal external kink or kink-ballooning mode produced by MISHKA is not corrected. Although this is usually acceptable, the perturbative approach has been shown to over-predict stability [31, 53].

Firstly it is interesting to see how changes in the fast ion distribution function affect the contribution of energetic ions to δW_K since the density scan performed in the MAST experiments had the effect of altering f_h significantly, as described in section 3. It is evident from equation 7 that the change in the potential energy of the mode depends upon the gradient of the distribution function with respect to energy and radius. As well as directly affecting the $\partial f_j/\partial\mathcal{E}$ and $\partial f_j/\partial\psi$ terms, changing $f_j(\mathcal{E},\psi)$ also affects the particles in resonance with the Doppler-shifted mode frequency due to changes in both the orbit frequencies of the particles and the local plasma rotation at different radii. In order to illustrate how the radial distribution affects the fast ion contribution to mode stability, the NBI ions are assumed to be described by a non-symmetric distribution slowing down in energy, Gaussian with respect to radius and pitch angle [56]:

$$f_h^p = C\exp\Big[\frac{\psi-\psi_0}{\Delta\psi}\Big]\exp\Big[\frac{\lambda-\lambda_0}{\Delta\lambda}\Big]\frac{1}{\mathcal{E}^{3/2}+\mathcal{E}_c^{3/2}}\mathrm{Erf}_c\Big[\frac{\mathcal{E}-\mathcal{E}_0}{\Delta\mathcal{E}}\Big] \tag{9}$$

where $\Delta\psi = 0.1$, $\lambda_0 = 0.5$, $\Delta\lambda = 0.5$, $\mathcal{E}_0 = 80$keV, $\mathcal{E}_c = 3$keV and $\Delta\mathcal{E} = 3.5$keV. Consequently, the deposition location, ψ_0, of the fast ions can be altered whilst keeping the equilibrium unchanged. Figure 11 shows how δW_K varies as ψ_0 and $\mathcal{E}_0$ are varied, which effectively moves the peak of the distribution function radially, and changes the birth energy of the slowing-down distribution in energy space respectively. When ψ_0 is varied to move the radial location of the peak of the fast ion distribution function,

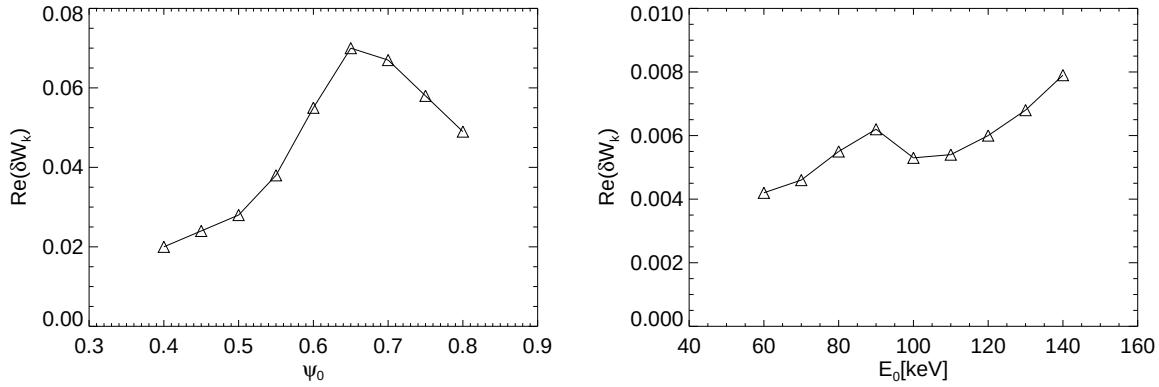

Figure 11. The change in the kink mode potential energy as (a) the peak of the distribution function is moved radially and (b) the peaking of the distribution function in energy space is varied.

the change in the potential energy of the mode is increased as the distribution function aligns with the eigenfunction of the unstable mode. In this case, the slowing down distribution has $\mathcal{E}_0 = 80$keV and the external kink eigenfunction is taken from an actual MAST plasma, and as such exhibits a rather global structure. It is clear that for the fast ions to play a significant role they must be well confined near the edge of the plasma, and this would be exacerbated if the eigenfunction was more edge-localised. As the energy is varied, the fast ion damping also varies. In this scan, the birth energy of the slowing down distribution, $\mathcal{E}_0$ is varied. Whilst in general more energetic ions have a stronger effect since their orbit widths are larger, there is some structure when the proportion of the distribution function with a precession frequency near the Doppler-shifted mode frequency, here taken from MAST plasma 25109 as described in section 3, is maximised. In principle, the pitch angle distribution also strongly affects δW_K [28]; if the trapped fraction increases, typically the stabilising effect on the RWM also increases. That said, however, the distribution of the beam ions with respect to $v_\parallel/v$ does not vary significantly as the density changes.

As figure 9 shows, the variation in plasma density also has a marked effect on the plasma rotation. The effect of varying the plasma flow on the kinetic damping has been analysed by taking a fixed distribution of beam ions given by expression 9 and varying $\omega - \omega_E$. It is clear that the change in the potential energy of the mode resulting from the presence of thermal ions has a strong dependence upon velocity. This is intuitively understood (and reported previously [28–30]) as equation 7 is maximised when the denominator approaches zero. This happens for the thermal ions in figure 12 when the mode frequency is in resonance with $\omega_{d,th}$ or $\omega_{b,th}$. Whilst δW_k arising from thermal ions strongly depends on the rotation, the fast ion response is an almost constant small increment, increasing slightly as the mode frequency approaches $\omega_{d,h}$ at high plasma flows. Similar results have been reported for NSTX [57] and DIII-D [58] high-β plasmas. Whilst the effect of the fast ions only makes a comparatively small

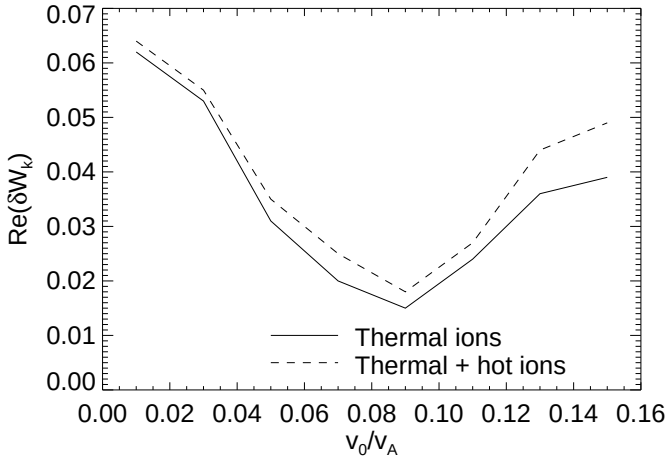

Figure 12. The real part of the change in the potential energy of the mode due to the kinetic response of the thermal ions and energetic beam ions with respect to the plasma frequency.

contribution to damping the mode, it can significantly impact the critical rotation at which the RWM is marginally stable, especially when the thermal ion response is far from a resonance.

4.2. Damping rates in MAST experiments

By calculating δW_k from both thermal and energetic ions for four different density MAST plasmas, the damping rate found numerically can be compared to the plasma response measured experimentally. The equilibria are reconstructed above both the RFA limit and the no-wall limit found using MISHKA-1. The beam ion distribution functions are taken from TRANSP simulations for each equilibrium. For any fixed distribution of beam ions, the stabilising effect of the fast particles scales with the energetic particle pressure. As can be seen in table 1 the contribution of the NBI ions to the total plasma pressure varies by a factor of six over this scan, and this strongly influences how different fast ion populations affect the RWM.

At high plasma density, the rotation is sufficiently large that the Doppler shifted mode frequency approaches the beam ion drift precession frequency. However, the low fast ion beta (where δW_K scales with β_h) coupled with increased collisionality (which slows down the beam ions more rapidly as seen in figure 8) means that the NBI ions do not strongly damp the RWM. Conversely, at very low density, the high fast ion fraction, increased effective orbit width effects and low plasma rotation result in enhanced fast ion stabilisation. As $v_0/v_A \to 0.01$, $\omega - \omega_E$ has a strong resonance with the precession frequency of the thermal ions too, significantly increasing δW_K. Indeed, even though the fast ion contribution is strongest at low density, the resulting low rotation means that the thermal ion stabilisation dominates the kinetic damping of the RWM, as illustrated

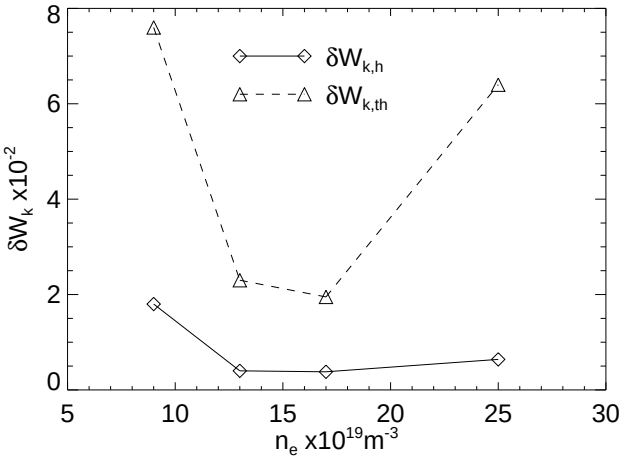

Figure 13. The potential energy of the mode due to the presence of energetic ions $\delta W_{k,h}$ and thermal ions $\delta W_{k,th}$ calculated by HAGIS for four different density MAST plasmas and respective distribution functions.

in figure 13. The RWM is least stable at intermediate densities, where corresponding intermediate rotation avoids resonance with either the thermal or fast ion precession frequency or the thermal bounce frequency.

By using equation 5, the damping/growth rate of the RWM can be found for four different density MAST plasmas. Figure 14 shows the growth rate of the mode as a function of $c_\beta = (\beta - \beta_{nowall})/(\beta_{wall} - \beta_{nowall})$ for a high density MAST plasma (shot 25109, $n_e = 6.8\times10^{19}m^{-3}$) and a low density case (discharge 25045, $n_e = 3.1\times10^{19}m^{-3}$). It is clear that the RWM is predicted to be stable to much higher β_N in the case of the low density. This is due in part to the enhanced fast ion stabilisation arising from the high β_h, but primarily from the low rotation which enhances the resonant contribution from the thermal ion precession frequency. Conversely, at high density, the RWM stability limit is much lower, though the thermal ion response still incurs a 30% increase in the β_N-limit. At intermediate densities, the non-resonant kinetic effects only result in weak stabilisation of the RWM.

Finally, it is possible to compare the damping rate of the RWM predicted by the drift-kinetic calculations presented here to the experimentally observed plasma response. Figure 15 shows the RWM damping rate at $c_\beta = 0.2$, for which the mode is predicted to be stable for all densities due to the kinetic damping. Correspondingly, the RWM is not observed in the MAST shots at the time at which these equilibria were reconstructed. Also shown for comparison is the plasma response according to equation 2. It is clear that the numerical simulations qualitatively recover the experimental results in predicting weakest stabilisation of the mode at intermediate densities. The damping is weakest for such mid-densities because the rotation of the plasma is such that the mode frequency is not near resonance with the thermal ion precession or bounce frequencies, as also observed in NSTX [30]. Furthermore, the fast ion response is also minimised

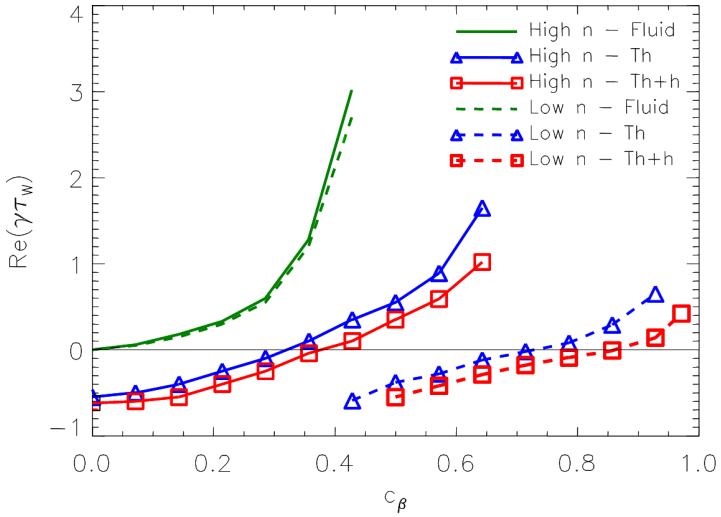

Figure 14. The growth/damping rate of the RWM for high and low density MAST plasmas with respect to $c_\beta = (\beta - \beta_{nowall})/(\beta_{wall} - \beta_{nowall})$. The damping is stronger for low density. In both cases thermal kinetic effects dominate the NBI contribution.

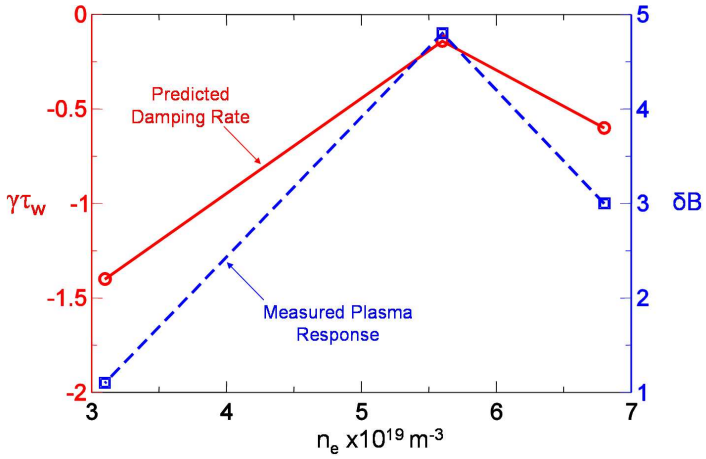

Figure 15. The damping rate of the resistive wall mode at $c_\beta = 0.2$ as a function of plasma density. Also shown for comparison is the measured plasma response in the MAST shots for the same time as the equilibria used in the simulations.

at such intermediate densities since the rotation frequency is not sufficiently large as to approach the fast ion precession frequency and the fast ion beta is not sufficiently large to give rise to a significant resistance to the perturbation.

5. Conclusions

Dedicated experiments have been performed in MAST to vary the fast ion distribution in both radial and velocity space as well as significantly in fast ion density so that $\beta_h/\beta_{total} \in [0.1, 0.6]$. Whilst the damping of the RWM due to the fast ions does change

over this scan, the dominant passive stabilisation of the mode allowing operation well above the no-wall limit arises from thermal ion effects. The strongest mode damping occurs when the plasma density is reduced since this has the effect of reducing the plasma rotation such that the Doppler-shifted mode frequency approaches a resonance with the thermal ion precession frequency. The fast ion effect is also maximised at low density since it scales with the fast ion fraction, which is maximised. At high rotation frequencies, resonance with both the beam ion precession frequency and thermal ion bounce frequency lead to significant damping of the mode. The RWM is predicted to be most unstable at intermediate densities, where kinetic effects are non-resonant, though still permit operation above the no-wall limit. The plasma response of applied oscillating fields is stronger for intermediate densities, in qualitative accordance with the predicted diminished mode damping.

The fact that passive stabilisation arising from both the thermal and energetic ions is strongly dependent upon the plasma rotation has significant implications for optimisation of operating regimes in present and future devices. In MAST, access to very fast rotation speeds which exceed the fast ion precession frequency, or approach the fast ion bounce frequency, are possible. However, such plasmas are heated by neutral beam injection on-axis, which has the secondary effect of stabilising sawtooth oscillations and precluding operation above the no-wall limit. Following an upgrade to MAST [59], additional complementary off-axis beams will provide the necessary non-inductive current drive to keep the safety factor above one and access high β_N strongly-rotating plasmas. In this case, the rotation profile may be tailored in order to maximise the resonance with the ensemble-averaged fast ion precession frequency, or indeed with the thermal ion bounce frequency. This has potentially beneficial implications for the operability of an ST-based components test facility or spherical tokamak power plant [60] above the no-wall β-limit.

The effect of energetic ions in DIII-D has been reported to be stronger than that observed in these MAST plasmas [58]. This is likely to be because the fast ion confinement near the edge of the plasma is relatively poor in these MAST plasmas due to a combination of the large orbit widths and the low plasma current (employed to maximise β_N). Since the RWM eigenfunction is largest near the plasma edge, the resonant stabilisation of the mode requires a significant fast ion population confined in this region, which is not the case in these MAST plasmas but is in DIII-D.

Acknowledgments

This work was funded partly by the RCUK Energy Programme under grant EP/I501045 and the European Communities under the contract of Association between EURATOM and CCFE. The views and opinions expressed herein do not necessarily reflect those of the European Commission. This work was carried out within the framework of the European Fusion Development Agreement.

References

[1] D Maisonnier et al, 2006 *Fus. Eng. Design* **81** 1123
[2] M Shimada et al, 2007 *Nucl. Fusion* **47** S1
[3] DJ Campbell et al, 2006 *21st IAEA Fusion Energy Conference, Chengdu* FT/1-1
[4] Becoulet A and Hoang GT, 2008 *Plasma Phys. Control. Fusion* **50** 124055
[5] Litaudon X et al, 2007 *Plasma Phys. Control. Fusion* **49** B529
[6] Joffrin E, 2007 *Plasma Phys. Control. Fusion* **49** B629
[7] Doyle EJ et al, 2006 *Plasma Phys. Control. Fusion* **48** B39
[8] Taylor TS 1997 *Plasma Phys. Control. Fusion* **39** B47
[9] RJ Bickerton et al, Nat. Phys. Sci., 229 (1971) 110
[10] Manickam J et al, 1994 *Phys. Plasmas* **1** 1601
[11] Manickam J et al, 1987 *Nucl. Fusion* **27** 1461
[12] Strait EJ *et al* 1995 *Phys. Rev. Lett.* **74** 2483
[13] Hender TC *et al* 2006 *21st IAEA Fusion Energy Conference, Chengdu, China* **EX/P8-18**
[14] Sabbagh SA *et al* 2006 *Nucl. Fusion* **46** 635
[15] Garofalo AM *et al* 1999 *Phys. Rev. Letters* **82** 3811
[16] Garofalo AM *et al* 2002 *Phys. Plasmas* **9** 1997
[17] La Haye RJ *et al* 2004 *Nucl. Fusion* **44** 1197
[18] Sontag AC *et al* 2005 *Phys. Plasmas* **12** 056112
[19] Reimerdes H *et al* 2006 *Phys. Plasmas* **13** 056107
[20] Reimerdes H *et al* 2007 *Phys. Rev. Lett.* **98** 055001
[21] Takechi M *et al* 2007 *Phys. Rev. Lett.* **98** 055002
[22] Strait EJ *et al* 2007 *Phys. Plasmas* **14** 056101
[23] Sabbagh SA *et al* 2010 *Nucl. Fusion* **50** 025020
[24] Bondeson A and Ward DJ 1994 *Phys. Rev. Lett.* **72** 2709
[25] Chu MS *et al* 1995 *Phys. Plasmas* **2** 2236
[26] Hu B, Betti R and Manickam J 2005 *Phys. Plasmas* **12** 057301
[27] Hu B and Betti R 2004 *Phys. Rev. Lett.* **93** 105002
[28] Chapman IT *et al* 2009 *Plasma Phys. Control. Fusion* **51** 055015
[29] Liu YQ, Chapman IT, Chu MS and Hender TC, 2008 *Phys Plasmas* **15** 112503
[30] Berkery J *et al* 2010 *Phys. Rev. Lett.* **104** 035003
[31] Liu YQ 2010 *Nucl. Fusion* **50** 095008
[32] Berkery J *et al* 2010 *Phys. Plasmas* **17** 082504
[33] Chapman et al, 2010 *Nucl Fusion* **50** 045007
[34] Reimerdes H *et al* 2004 *Phys. Rev. Lett.* **93** 135002
[35] Boozer AH 2001 *Phys. Rev. Lett.* **86** 5059
[36] Liu YQ, Chapman IT, Saarelma S, Gryaznevich MP, Hender TC and Howell DF 2009 *Plasma Phys. Control. Fusion* **51** 115005
[37] Chapman IT *et al* 2009 *Phys. Plasmas* **16** 072506
[38] Chapman IT 2011 *Plasma Phys. Control. Fusion* **53** 013001
[39] Chapman IT *et al* 2010 *submitted Nuclear Fusion* "Macroscopic stability of high beta MAST plasmas"
[40] Mikhailovskii AB, Huysmans GTA, Sharapov SE and Kerner WO 1997 *Plasma Phys. Rep.* **23** 844
[41] Gryaznevich MP *et al* 2008 *Plasma Phys. Control. Fusion* **50** 124030
[42] Huysmans G, Goedbloed J and Kerner W 1991 *Proceedings of the CP90 Conference on Computer Physics, Amsterdam*, (World Scientific, Singapore), p. 371
[43] Lao L *et al* 1990 *Nucl. Fusion* **30** 1035
[44] Budny R *et al* 1992 *Nucl. Fusion* **32** 429
[45] Liu YQ *et al* 2005 *Nucl. Fusion* **45** 1131
[46] Zheng LJ, Kotschenreuther MT and Van Dam JW 2010 *Phys. Plasmas* **17** 056104

[47] Kessel CE, Mau TK, Jardin SC and Najmabadi F, 2006 *Fus. Eng. Design* **80** 63
[48] Chapman IT, Kemp R and Ward DJ 2010 *accepted Fus. Eng. Design*
[49] Betti R and Friedberg JP 1995 *Phys. Rev. Lett.* **74** 2429
[50] Pinches SD *et al* 1998 *Comput. Phys. Commun.* **111** 133 (Release Version 8.09)
[51] Haney SW and Friedberg JP 1989 *Phys. Fluids B* **1** 1637
[52] Breizman BN, Candy J, Porcelli F and Berk H 1998 *Phys. Plasmas* **5** 2326
[53] Liu YQ *et al* 2008 *Phys. Plasmas* **15** 112503
[54] Chapman IT *et al* 2010 *Nucl. Fusion* **50** 045007
[55] Poli E *et al* 2008 *Phys. Plasmas* **15** 032501
[56] Chapman IT *et al* 2008 *Plasma Phys. Control. Fusion* **50** 045006
[57] Sabbagh SA *et al* 2010 *23rd IAEA Fusion Energy Conference, Daejeon, Korea* **EXS/5-5**
[58] Reimerdes H *et al* 2010 *23rd IAEA Fusion Energy Conference, Daejeon, Korea* **EXS/5-5**
[59] Stork D *et al* 2010 *23rd IAEA Fusion Energy Conference, Daejeon, Korea* **ICC/P5-06**
[60] Hole MJ, Wilson HR, Abeysuriya R and Larson JW 2010 *Plasma Phys. Control. Fusion* **52** 125005